The International Journal of Biochemistry & Cell Biology 64 (2015) 265–276

Contents lists available at ScienceDirect

The International Journal of Biochemistry & Cell Biology

journal homepage: www.elsevier.com/locate/biocel

Downregulation of microRNA-451 in non-alcoholic steatohepatitis inhibits fatty acid-induced proinflammatory cytokine production through the AMPK/AKT pathway

Wonhee Hur[a], Joon Ho Lee[a], Sung Woo Kim[a], Jung-Hee Kim[a], Si Hyun Bae[a,b], Minhyung Kim[c], Daehee Hwang[c,d], Young Seok Kim[e], Taesun Park[f], Soo-Jong Um[g], Byoung-Joon Song[h], Seung Kew Yoon[a,b,*]

[a] The Catholic University Liver Research Center & WHO Collaborating Center of Viral Hepatitis, College of Medicine, The Catholic University of Korea, Seoul, Republic of Korea
[b] Department of Internal Medicine, Seoul St. Mary's Hospital, College of Medicine, The Catholic University of Korea, Seoul, Republic of Korea
[c] School of Interdisciplinary Bioscience and Bioengineering, POSTECH, Pohang, Republic of Korea
[d] Department of New Biology and Center for Plant Aging Research, Institute for Basic Science, DGIST, Daegu, Republic of Korea
[e] Department of Internal Medicine, Soon Chun Hyang University Hospital Bucheon, Soon Chun Hyang University College of Medicine, Bucheon, Republic of Korea
[f] Department of Food and Nutrition, Yonsei University, Republic of Korea
[g] Department of Bioscience and Biotechnology/Institute of Bioscience, Sejong University, Republic of Korea
[h] Laboratory of Membrane Biochemistry and Biophysics, National Institute on Alcohol Abuse and Alcoholism, Bethesda, MD, USA

ARTICLE INFO

Article history:
Received 12 January 2015
Received in revised form 16 April 2015
Accepted 28 April 2015
Available online 7 May 2015

Keywords:
Non-alcoholic fatty liver
Non-alcoholic steatohepatitis
MicroRNAs
MicroRNA-451
Cab39/MO25
Inflammation

ABSTRACT

Mechanisms associated with the progression of non-alcoholic fatty liver disease (NAFLD) remain unclear. We attempted to identify the pattern of altered gene expression at different time points in a high fat diet (HFD)-induced NAFLD mouse model. The early up-regulated genes are mainly involved in the innate immune responses, while the late up-regulated genes represent the inflammation processes. Although recent studies have shown that microRNAs play important roles in hepatic metabolic functions, the pivotal role of microRNAs in the progression of NAFLD is not fully understood. We investigated the functions of miR-451, which was identified as a target gene in the inflammatory process in NAFLD. miR-451 expression was significantly decreased in the palmitate (PA)-exposed HepG2 cells and in liver tissues of HFD-induced non-alcoholic steatohepatitis (NASH) mice. Its decreased expressions were also observed in liver specimens of NASH patients. *In vitro* analysis of the effect of miR-451 on proinflammatory cytokine provided evidence for negative regulation of PA-induced interleukin (IL)-8 and tumor necrosis factor-alpha (TNF-α) production. Furthermore, miR-451 over-expression inhibited translocation of the PA-induced NF-κB p65 subunit into the nucleus. Our result showed that Cab39 is a direct target of miRNA-451 in steatotic cells. Further study showed that AMPK activated through Cab39 inhibits NF-κB transactivation induced in steatotic HepG2 cells. miR-451 over-expression in steatotic cells significantly suppressed PA-induced inflammatory cytokine. These results provide new insights into the negative regulation of miR-451 in fatty acid-induced inflammation *via* the AMPK/AKT pathway and demonstrate potential therapeutic applications for miR-451 in preventing the progression from simple steatosis to severely advanced liver disease.

Abbreviations: AMPK, adenosine monophosphate activated protein kinase; DEGs, differentially expressed genes; GEO, gene expression omnibus; GOBPs, gene ontology biological processes; IL, interleukin; miRNAs, microRNAs; NAFLD, non-alcoholic fatty liver disease; NASH, non-alcoholic steatohepatitis; NF-κB, nuclear factor kappa-light-chain-enhancer of activated B cells; PA, palmitate; qRT-PCR, quantitative real-time reverse transcriptase-polymerase chain reaction; TNF-α, tumor necrosis factor-alpha.

* Corresponding author at: Department of Internal Medicine, Seoul St. Mary's Hospital, College of Medicine, The Catholic University of Korea, Banpo-daero 222, Seocho-gu, Seoul, Republic of Korea. Tel.: +82 2 2258 7534; fax: +82 2 536 9559.
E-mail addresses: wendyhur@catholic.ac.kr (W. Hur), JoonHo@catholic.ac.kr (J.H. Lee), never-i@nate.com (S.W. Kim), kim.jh@catholic.ac.kr (J.-H. Kim), baesh@catholic.ac.kr (S.H. Bae), hyung926@postech.ac.kr (M. Kim), dhwang@dgist.ac.kr (D. Hwang), liverkys@schmc.ac.kr (Y.S. Kim), tspark@yonsei.ac.kr (T. Park), umsj@sejong.ac.kr (S.-J. Um), bj.song@nih.gov (B.-J. Song), yoonsk@catholic.ac.kr (S.K. Yoon).

http://dx.doi.org/10.1016/j.biocel.2015.04.016

1. Introduction

Non-alcoholic fatty liver disease (NAFLD) with accumulated fat in the liver is a common cause of chronic liver disease in Western countries (Lewis and Mohanty, 2010; Ogawa et al., 2014). NAFLD comprises a diverse spectrum of manifestations, ranging from simple steatosis to steatohepatitis, fibrosis and cirrhosis (Nguyen and Sanyal, 2012). A subset of individuals with NAFLD progress to decompensated liver diseases and liver cancer (Pais et al., 2013). The recent increasing prevalence of NAFLD is considered to be related to the epidemic of obesity and type 2 diabetes in the USA and other developed countries (Bellentani and Marino, 2009). In addition, NAFLD is reported to be strongly associated with metabolic syndrome including hypertension and cardiovascular disease and it is therefore regarded as a clinical manifestation of complex metabolic disease spectrum in the liver (Targher et al., 2010). For this reason, it is necessary to actively investigate the underlying disease mechanism to manage the individuals with NAFLD more effectively.

A "two-hit hypothesis" was initially proposed to explain the pathogenesis and progression of NAFLD (Day and James, 1998). However, recent investigations have provided evidence that 'multiple hits' of multiple factors are involved in the pathogenesis and progression of NAFLD (Tilg and Moschen, 2010). These hits execute the occurrence of parallel events of a complex interplay among host genetics, environmental risk factors and, the gut microbiota (Bechmann et al., 2012). Such interactions can cause isolated hepatic steatosis, innate immune activation, inflammation, apoptosis and/or progressive liver damage (Tilg and Moschen, 2010). Although considerable progress has been made recently in elucidating the pathogenesis of NAFLD, it remains unclear how the inflammatory mediators are involved in the progression of NAFLD. To investigate the molecular mechanisms underlying the progression of NAFLD, it is essential to develop appropriate *in vitro* and *in vivo* models. We previously established a high fat diet (HFD)-induced NAFLD mouse model that exhibits pathological features similar to those in humans (Kim et al., 2014). In addition, we developed an *in vitro* model of hepatocytic steatosis in a HepG2 cell line exposed to palmitate (PA). We also showed the preventive and therapeutic effects of oleuropein, a secoiridoid derived from olives (*Olea europaea*), on the progression of hepatic fibrosis from steatohepatitis in these experimental models (Hur et al., 2012; Kim et al., 2014; Park et al., 2011).

MicroRNAs (miRNAs) represent a class of small non-coding RNAs involved in various biological processes, including cell proliferation, development and differentiation (Shukla et al., 2011).

Recent studies have demonstrated that miRNAs play important roles in the control of energy, and hepatic metabolic functions regulating fatty acid (FA) and cholesterol metabolism in NAFLD (Alisi et al., 2011; Ceccarelli et al., 2013). Of the many differentially expressed miRNAs between steatosis and nonalcoholic steatohepatitis (NASH), we focused miRNA (miR)-451 and studied the role of miR-451 in the progression of NAFLD to NASH.

miR-451 is known to exert various biological functions in cancer, infectious disease, cardiovascular and metabolic diseases. Previous studies have revealed that the dysregulation of miR-451 expression is involved in carcinogenesis and in tumor progression by affecting cell proliferation, cell-cycle distribution, migration, and invasion (Li et al., 2013; Liu et al., 2013; Tian et al., 2012). Furthermore, a recent study showed that miR-451 regulates dendritic cell cytokines and suppresses neutrophil chemotaxis *via* down-regulation of p38 MAPK phosphorylation (Murata et al., 2014; Rosenberger et al., 2012). Specifically, the effects of miR-451 are mediated by the liver kinase B1 (LKB1)/5′-adenosine monophosphate activated protein kinase (AMPK) pathway, which controls key players in metabolic pathways and thus emerges as a major regulator of glucose and lipid metabolism with multiple beneficial roles in the target tissues (Godlewski et al., 2010). However, the expression and function of miR-451 in NAFLD are still unclear and the molecular mechanisms underlying the progression to NASH from simple steatosis have yet to be elucidated. Our study aimed to investigate the role of miR-451 in the molecular mechanisms of the pathogenic procession of NAFLD. We found that miR-451 expression was downregulated in the livers of HFD-induced NASH mice and that miR-451 regulates inflammatory cytokine secretion from steatotic cells through the AMPK, Akt and NF-κB singling pathways *via* direct targeting of Cab39.

2. Materials and methods

2.1. Animals and diets

Five-week-old male C57BL/6 mice were purchased from Orient Bio (Seoul, South Korea) and housed in a standard animal facility under a 12:12-h light–dark cycle with a constant room temperature. The mice were divided into four weight-matched groups. Mice were fed either a normal diet (ND) of 3.8 kcal/g (ND; 50.21% carbohydrate, 20.78% protein and 4.8% fat) or high fat diet (HFD: D12231, Research Diets, Inc., New Brunswick, NJ) of overall 5.2 kcal/g (25.5% carbohydrate, 16.4% protein and 58% fat) for 3 months or 9 months *ad libitum*. Food intake was measured by weighing the pellets once per week. All animals were cared for according to institutional guidelines, and all experiments were approved by the Institutional Animal Care and Use Committee at the Catholic University of Korea. In all experiments, each group consisted of at least 3–4 mice.

2.2. Hepatic pathological evaluation

Fresh liver tissue samples were fixed in 3.7% buffered formalin, and then embedded in paraffin wax. Liver pathology was assessed by hematoxylin-eosin (H&E) and Oil Red O staining of liver sections for evaluation of steatosis, fat droplets and inflammation. All stained slides were scored by two experienced pathologists and graded by a previously described classification (Jeen and Jin, 2009).

The degree of steatosis was graded on a four-point scale: grade 0, steatosis in <5% of hepatocytes; grade 1, steatosis in up to 33%; grade 2, steatosis in 33–66%; grade 3, steatosis in >66% of hepatocytes. Lobular inflammation was also graded on a four-point scale: grade 0, no foci; grade 1, fewer than two foci per 20× field; grade 2, two to four foci per 20× field; grade 3, more than four foci per 20× field. Hepatocyte ballooning was graded on a three-point scale: 0, none; 1, a few balloon cells; 2, many/prominent balloon cells. For the NAFLD activity score (NAS), features of steatosis, lobular inflammation, and hepatocyte ballooning were combined, and the range was scored from 0 to 8. Cases scoring ≥5.0 were diagnosed as NASH, while cases ≤2 were diagnosed as simple steatosis.

2.3. mRNA microarray experiments

Total RNAs were prepared independently from liver tissues of two different mice for each condition (3 month-HFD, 9 month-HFD and control) using the RNeasy mini kit (Qiagen, Hilden, Germany). RNA integrity was assessed using an Agilent 2100 Bioanalyzer. RNA integrity numbers for all samples were above 8.5. RNA was then reverse-transcribed, amplified and hybridized to the Agilent SurePrint G3 mouse GE 8X60K microarray according to the Agilent's protocols. The probe intensities were obtained using the Agilent G2565BA microarray scanner and normalized using the quantile normalization method (Bolstad et al., 2003). The microarray data were deposited in the gene expression omnibus (GEO) database (accession ID: GSE59042).

2.4. Statistical analysis of gene expression data

Comparisons (control *versus* 3 month-HFD and control *versus* 9 month-HFD) were conducted to identify differentially expressed genes (DEGs) using the integrative statistical method previously reported (Chae et al., 2013). Briefly, for each mRNA, an adjusted *P*-value was computed by performing the two-tailed *T*-test and log2 median ratio test using the empirical distributions estimated by random permutations of the samples. The two sets of *P*-values from the individual tests were combined to compute the overall *P*-values using Stouffer's method (Hwang et al., 2005). Finally, the DEGs were selected for genes with (1) $P \leq 0.05$ and (2) absolute log2-fold-changes ≥ 0.58 (1.5-fold). Enriched GO biological process genes were identified as the ones with $P < 0.05$ using DAVID software (Huang da et al., 2009).

2.5. Quantitative real-time reverse transcriptase-polymerase chain reaction (qRT-PCR)

Total RNA was isolated from pooled mouse livers in each group using the RNeasy Plus Mini kit (Qiagen). MicroRNA was prepared as described above. The qRT-PCR for miRNAs was performed using the Mir-X™ miRNA First-Strand Synthesis Kit and SYBR Advantage qPCR Premix (Clontech, Mountain View, CA) on an Applied Biosystem 7500 Fast system (Applied Biosystems) according to the manufacturer's instructions. Relative expression of each miRNA was normalized to the U6 snRNA (ΔCT) in each sample. Quantitative expression of a given miRNA was compared to the internal control and determined according to the CT method ($2^{-\Delta\Delta Ct}$) (Livak and Schmittgen, 2001).

2.6. Cell culture and siRNA/miRNA transfection

HepG2 cells (American Type Culture Collection, Manassas, VA) were grown in minimum essential medium (MEM; Invitrogen, Carlsbad, CA) supplemented with 10% fetal bovine serum (FBS), 100 μg/ml penicillin, and 0.25 μg/ml streptomycin at 37 °C in a humidified incubator with 5% CO_2. Fatty acid-free bovine serum albumin (1%; Sigma–Aldrich, St. Louis, MO) was used as a vehicle for PA treatment. After reaching 70% confluence, cultured cells were serum-starved and exposed to 0.5 mM PA in medium containing 1% FFA-free BSA.

Cells were transfected with *hsa-miR-451mimic* (Genolution Pharmaceuticals, Seoul, Korea), Cab39 siRNA, or scrambled miRNA (Genolution) as a negative control using G-fectin (Genolution) according to the manufacturer's instructions at a final concentration of 30 nM. All transfections were carried out in duplicate or triplicate.

2.7. Immunoprecipitation and western blot analysis

Immunoprecipitation was performed as previously described (Godlewski et al., 2010). Following treatment, cells were washed and lysed in protein extraction buffer containing 20 mM Tris (pH 7.5), 150 mM NaCl, 10% glycerol, 1% Triton X-100, 2 mM EDTA, 1 mM phenylmethylsulfonyl fluoride, and Complete Protease Inhibitor Cocktail (Roche, Mannheim, Germany). Lysates were cleared by centrifugation, and the protein content was determined using a Bradford protein assay kit (Bio-Rad, Hercules, CA). Cell lysates were separated by 12% SDS-polyacrylamide gel electrophoresis and transferred to nitrocellulose membranes (Whatman, Maidstone, Kent, UK). The membranes were incubated overnight at 4 °C with the following primary antibodies against β-actin, Cab39/MO25, AMPK, phospho-AMPK, p65 (RelA), phospho-IκBα, STRAD, LKB1, OGT, or Ywhaz. After overnight incubation, membranes were washed three times with Tris-buffered saline containing 0.05% Tween-20 and incubated with horseradish peroxidase-conjugated anti-mouse, anti-rabbit or anti-goat secondary antibodies (Amersham Pharmacia Biotech, Piscataway, NJ). Protein bands were visualized using an enhanced chemiluminescence system (Amersham Pharmacia Biotech) according to the manufacturer's instructions. Protein band densities were determined by densitometry analysis (NIH Image J software, Bethesda, MA).

2.8. Cell fractionation and immunofluorescence staining

Transfected HepG2 cells were fractionated into nuclear fractions using a NE-PER kit (Pierce, Rockford, IL).

For immunofluorescence staining, transfected cells were fixed, incubated with anti- NF-κB p65 mouse monoclonal (Cell Signaling) antibodies, followed by incubation with Alexa 594-labeled anti-mouse IgG (1:500; Jackson ImmunoResearch Laboratories, Inc., West Grove, PA). Cells were stained with DAPI (Sigma) to counterstain the nuclei and then examined using fluorescence microscopy (Carl Zeiss, Oberkochen, Germany).

2.9. Luciferase reporter assays

Cells (5×10^5/well) were seeded in triplicate wells in six well plates. One hundred nanograms of pNF-κB luciferase plasmid or pGL3 luciferase plasmid (control-luciferase plasmid) plus 10 ng pRL-TK *Renilla* plasmid (Promega, Madison, WI) were transfected into cells using the Lipofectamine 2000 reagent (Invitrogen). Two days after transfection, the luciferase activity was measured using the Dual Luciferase Reporter Assay Kit (Promega) according to the manufacturer's protocol. The firefly luminescence signal was normalized to the *Renilla* luminescence signal. Three independent experiments were performed and data are presented as the mean ± SD.

2.10. Quantitation of cytokine concentration in supernatants from cultured cells using ELISA

The transfected HepG2 cells were grown in triplicates and stimulated with 0.5 mM PA in MEM containing 1% FFA-free BSA. Conditioned medium was saved and stored at −70 °C until use. The amount of IL-8 and TNF-α released into culture supernatants was quantified by using a human IL-8 and TNF-α Quantikine ELISA Kit according to the manufacturer's instructions (R&D Systems, Minneapolis, MN). The absorbance at 450 nm was determined on an ELISA reader (Laboratory systems, iEMS Reader MF, Copenhagen, Denmark).

2.11. Statistical analysis

All data are represented as means ± standard error of at least three separate experiments. The Student's *t*-test for unpaired two groups was executed using SPSS (IBM, New York). Differences were considered statistically significant at $P < 0.05$ or $P < 0.001$.

3. Results

3.1. Alteration of inflammation-related gene expression in the livers of HFD-induced NAFLD mice

Mechanisms associated with the progression of simple steatosis to steatohepatitis in NAFLD remain undefined. Understanding the molecular mechanisms underlying the process of NAFLD is essential in designing rational treatment strategies.

First, to determine how gene expression is altered between NAFLD and NASH, we performed the gene expression profiles in liver tissues from HFD-induced NAFLD mice compared to those from ND-fed mice using Agilent SurePrint G3 mouse microarray

platforms. The NAFLD mouse model was established successfully after feeding a 58% HFD for 3 months (NAFLD) and 9 months (NASH) and confirmed by an independent pathologist. Our treatment result was consistent with previous reports (Kim et al., 2014). This was determined by H&E (Fig. 1A) and Oil Red O (Fig. 1C) staining, which revealed that simple steatosis occurred at 3 months with various degrees of fat deposition. At 9 months, the disease progressed to NASH with more severe steatosis, numerous ballooning hepatocytes and mild to moderate lobular inflammation (Fig. 1B).

To identify potential molecular pathways involved in NAFLD progression, we then compared mRNA expression levels in HFD-induced NAFLD mice (3 or 9 months) compared to those in ND-fed mice. We identified a total of 2362 DEGs (with 1485 and 1597 at 3 and 9 months, respectively) using a previously reported statistical method (Section 2). Based on the differential expression of those genes, 2362 DEGs were further categorized into eight clusters (Supplementary Table S1). We focused on six major clusters (C1–6; Fig. 1D) with more than 118 genes (5% of the total number of DEGs). To understand the cellular processes represented by the genes in individual clusters, we performed an enrichment analysis of Gene Ontology biological processes (GOBPs) for the genes in each cluster (Fig. 1E right). The early up-regulated genes at 3 months (C1–2) are mainly involved in processes related to innate immune response (antigen processing and presentation, cell adhesion, leukocyte differentiation, cell proliferation, and lipid transport), indicating early activation of these immune processes. Some of these processes (antigen processing and presentation, cell adhesion and lipid transport), represented by C1, showed sustained activations at 9 months, while others, represented by C2, were restored back to basal levels. Importantly, the late up-regulated genes at 9 months (C3) are involved in other inflammation related processes (blood coagulation, lipid synthesis and metabolic processes, regulation of angiogenesis, ion homeostasis, and cell migration), indicating severe and systematic inflammation. In contrast, the down-regulated genes are involved in processes in oxidative stress response, translation and cell proliferation.

Taken together, these results show that hepatic inflammation is one of the most distinguishing features of NASH and therefore more detailed insight in inflammation related processes in the progression of NAFLD is needed.

3.2. Expression of miR-451 is down-regulated in human NASH

The results of microarray analysis revealed that one of the genes differentially expressed between NAFLD and NASH is miR-451, which is known to be involved in cytokine production, cancer, infectious diseases, cardiovascular and metabolic diseases. To further determine the potential roles of miR-451 in the progression of NAFLD, we measured its hepatic expression in liver tissues in mouse models and human specimens with histologically confirmed NAFLD and NASH, respectively, by stem-loop RT-PCR. As shown in Fig. 2A, the levels of miR-451 were significantly decreased in the livers of HFD-induced NASH mice (at 9 months) compared with those in HFD-induced hepatic steatotic mice (at 3 months). Our results showed that the expression levels of miR-34a were significantly higher in NASH than simple steatosis (Fig. 2B). These results are consistent with the previous results (Castro et al., 2013, Pogribny et al., 2010), thus validating that our HFD-induced NAFLD and NASH models were appropriate for further characterization. We also examined the levels of miR-451 in human liver sections with NAFLD or NASH. Interestingly, the expression levels of miR-451 were significantly decreased in patients with NASH compared to simple steatosis (Fig. 2C).

These results suggest that miR-451 expression was down-regulated in the inflammatory progression of NAFLD in both animal models and human specimens.

3.3. miR-451 inhibits palmitate induced production of proinflammatory cytokines

A previous study showed that miR-451 regulated the production of cytokines by influenza-infected dendritic cells (Rosenberger et al., 2012). Based on this result, we examined the effect of miR-451 expression on pro-inflammatory cytokine production to determine whether miR-451 plays a role in regulating production of inflammatory cytokines partly responsible for the progression from simple steatosis to NASH. We first established a model of cellular steatosis by incubating HepG2 cells with PA in media containing FFA-free BSA (Fig. 2D) and measured the production of proinflammatory Cytokines, such as IL-8 and TNF-α as previously reported (Joshi-Barve et al., 2007; Manco et al., 2007).

As shown in Fig. 2E, miR-451 expression was significantly lower in HepG2 cells treated with PA than in cells treated with BSA alone. In addition, the expression level of miR-451 was significantly higher in HepG2 cells harboring ectopically expressed miR-451 than in the scrambled miRNA-transfected cells (miR-NC) ($P < 0.05$, Fig. 2F).

We next examined whether PA-induced secretion of IL-8 and TNF-α is negatively affected by miR-451 mimics. The ELISA result showed that PA-induced IL-8 and TNF-α expression was significantly decreased in miR-451-overexpressing HepG2 cells compared with miR-NC-transfected cells (Fig. 2G). However, IL-8 and TNF-α expression was not significantly different between miR-451-overexpressing HepG2 cells and miR-NC-transfected cells following treatment with BSA (Fig. 2G). These findings indicate that miRNA-451 expression can negatively regulate pro-inflammatory cytokine expressions in PA-exposed HepG2 cells.

Taken together, our results further demonstrate that miR-451 could modulate inflammatory cytokine production in the progression of NASH from simple steatosis.

3.4. miR-451 expression inhibits PA- induced NF-κB activation

Since IL-8 or TNFa expression activated by PA can be modulated by NF-kB as reported (Joshi-Barve et al., 2007; Wang et al., 2009), we further investigated whether miR-451 expression might modulate NF-kB activation in PA-exposed HepG2 cells. To this purpose, we co-transfected with luciferase-reporter constructs containing NF-kB binding motifs and miR-451 mimics into HepG2 cells. As expected, the expression of miR-451 mimicked significantly reduced PA-induced luciferase activity indicating an attenuation of NF-κB activation in PA-exposed HepG2 cells (Fig. 3A). However, there was no significant difference in luciferase activity between both groups of HepG2 cells treated with BSA alone.

Since NF-κB activation is usually mediated by the nuclear translocation of the NF-κB/Rel family of transcription factors, we examined the effect of miR-451 overexpression on the cytosolic and nuclear distribution of the NF-κB p65 subunit by Western blot analysis after transfection and PA or BSA treatment (Fig. 3B). We showed that PA treatment effectively increased the nuclear NF-κB p65 protein level and decreased the cytosolic NF-κB p65 protein level, which is an indication of the nuclear translocation of NF-κB p65 subunit. However, ectopic overexpression of miR-451 inhibited the PA-stimulated increase and decrease of the nuclear and cytosolic NF-κB p65 levels in HepG2 cells. We further determined whether miR-451 expression had any effect on IκB-α phosphorylation in PA-exposed HepG2 cells. As shown in Fig. 3C, PA treatment in HepG2 cell induced IκB-α phosphorylation and miR-451 expression in PA exposed cell inhibited PA-induced IκB-α phosphorylation.

An immunofluorescent staining analysis after PA treatment showed that the red fluorescence intensity from positive NF-κB p65 antibody staining in the nucleus was decreased in miR-451 overexpressing HepG2 cells compared with miR-NC transfected HepG2 cells (Fig. 3D and E). However, there was no significant difference

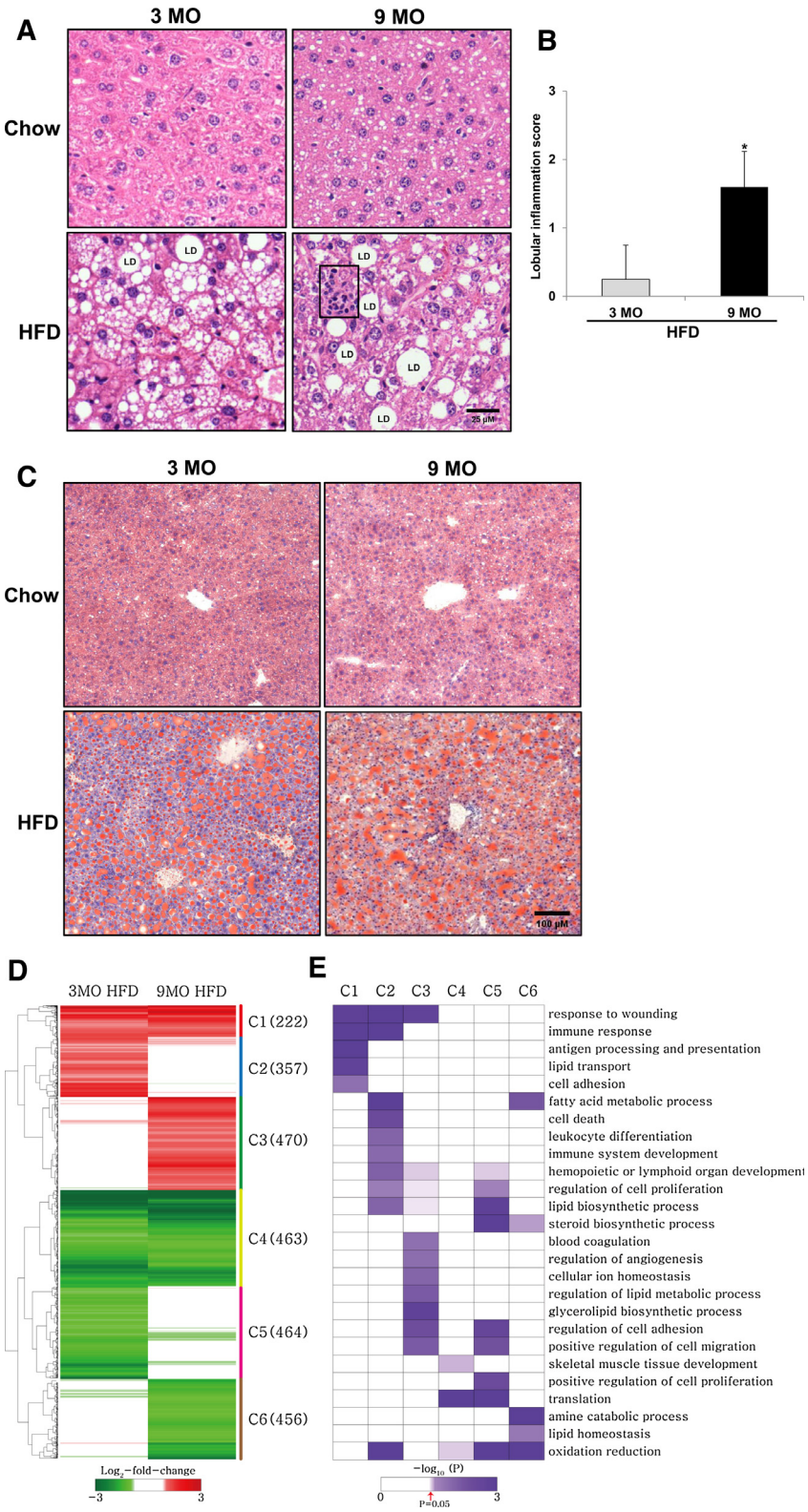

Fig. 1. Alteration of inflammation-related gene expression in the livers of HFD-induced NAFLD mice. (A) Representative H&E staining of hepatic sections (×400 object, scale bar = 25 μm). Livers from mice fed a normal diet (chow, $n = 8$) or HFD for 3 months (steatosis, $n = 4$) or 9 months (NASH, $n = 9$). The liver sections from mice fed HFD for 9 months (NASH) show deposition of large fat droplets (LD), infiltration of inflammatory cells (black box) and hepatocyte necrosis. Normal histology of liver sections is seen from mice fed on a normal diet. (B) The inflammation score of the mouse liver specimens is described in the "Materials and methods" section. $^*P < 0.05$ compared with 3 MO HFD. (C) Representative Oil red O staining for lipids in the livers of C57BL/6 mice fed a chow or HFD, as indicated (×150 object, Scale bar = 100 μm). (D) Heat map showing the six major clusters of the DEGs (C1–6). Red and green colors represent up- and down-regulation in HFD, respectively, compared to control. Numbers of the genes in clusters are denoted in parentheses. Color bar, gradient of $\log_2$-fold-changes. (E) Heat map showing the GOBPs represented by genes in C1–6. The color represents the significance (P-value) of the GOBPs being represented by the genes in C1–6. Color bar, gradient of $-\log_2(P)$, where P is the P-value computed using DAVID software. (For interpretation of the references to color in this figure legend, the reader is referred to the web version of the article.)

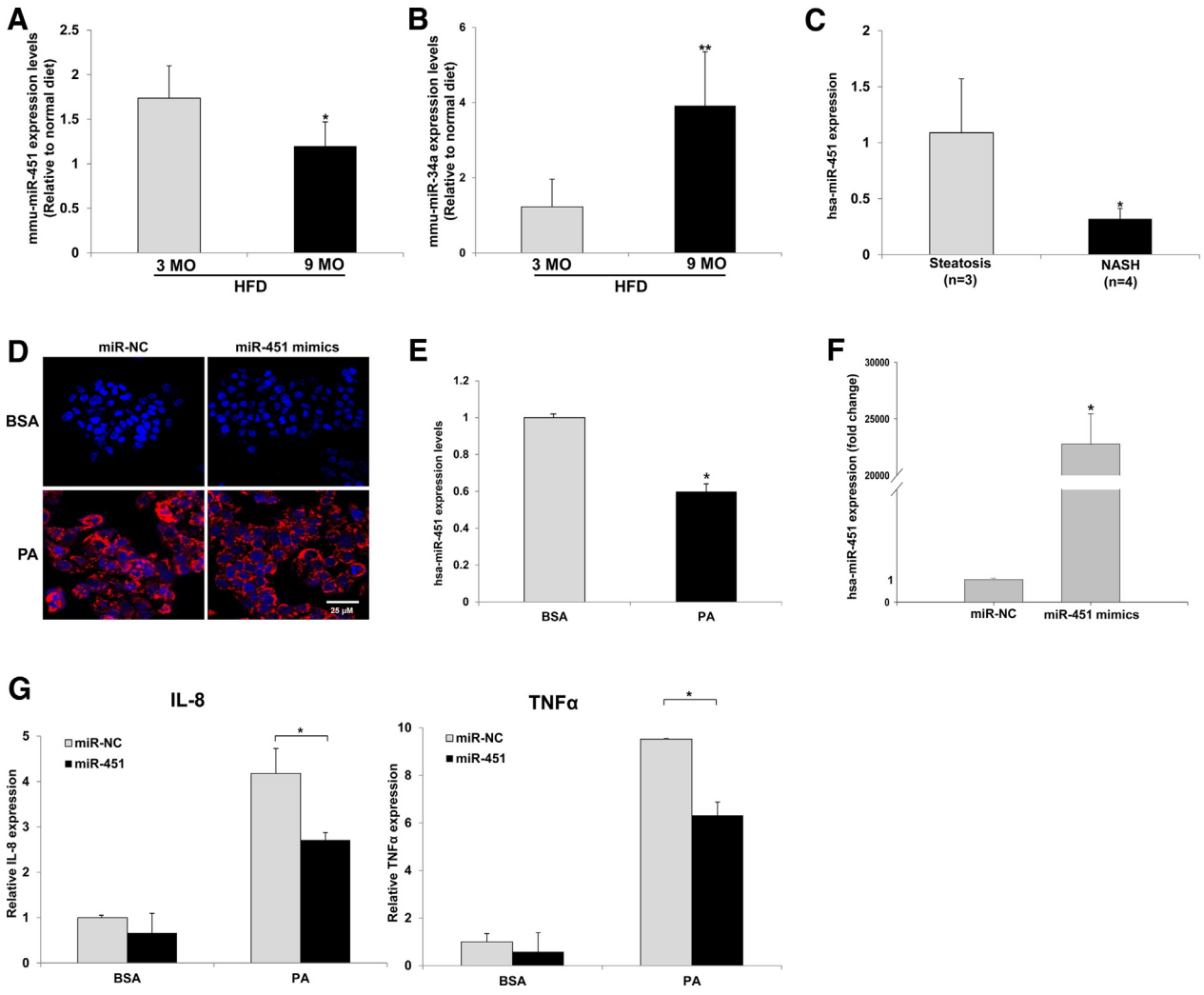

Fig. 2. Down-regulation of miR-451 expression negatively regulates IL-8 expression in HepG2 cells treated with PA. (A, B) miR-451 (A) and miR-34a (B) expression in liver tissue was measured from C57BL/6 mice fed with a normal diet ($n = 8$) or HFD for 3 months ($n = 4$) or 9 months ($n = 9$) by qRT-PCR. $^{*}P < 0.05$, $^{**}P < 0.001$ compared with 3 MO HFD. (C) Determination of miR-451 expression by qRT-PCR in biopsied livers of NASH patients ($n = 4$) compared to those with steatosis ($n = 3$). $^{*}P < 0.05$ compared with steatosis. (D) Representative fluorescence photomicrographs showing intracellular lipid accumulation in Nile Red-stained cells after transfection with miR-451 mimics in the presence of 0.5 mM PA. The nuclei were counterstained with DAPI (blue). Scale bar = 25 μm. (E) The miR-451 expression levels in cultured HepG2 cells treated with BSA or PA were determined by using qRT-PCR. $^{*}P < 0.05$ compared with BSA alone. (F) HepG2 cells were transfected with 30 nM of miR-NC or miR-451 mimics for 24 h. qRT-PCR analysis was performed 24 h after transfection to determine the miR-451 levels in HepG2-miR451 cells. $^{*}P < 0.05$ compared from miR-NC. (G) miR-451 overexpression suppressed PA-induced IL-8 and TNF-α secretion. miR-451 expressing HepG2 cells were treated with PA or BSA as indicated for 12 h followed by IL-8 and TNF-α expression measurement by ELISA. $^{*}P < 0.05$ compared from miR-NC. (For interpretation of the references to color in this figure legend, the reader is referred to the web version of the article.)

in positive NF-κB p65 antibody staining between both groups after BSA treatment. The results suggest that miR-451 overexpression regulates NF-kappaB pathway through inhibition of nuclear NF-κB p65 translocation *via* IκB-α phosphorylation

3.5. *miR-451 is a repressor of Cab39 translation*

Previous studies have demonstrated that miR-451 targets the 3′UTR mRNAs of Cab39 (Godlewski et al., 2010; Tian et al., 2012), OGT (Bergamaschi and Katzenellenbogen, 2012) and Ywhaz (Wu et al., 2013; Zhang et al., 2012) in multiple cell types. To confirm the expression of these target genes regulated by miR-451, qRT-PCR and Western blotting were performed with murine hepatic tissues. The OGT and Ywhaz protein levels remained unchanged between HFD-induced hepatic steatosis (3-months) and NASH (9-months) mice (Supplementary Fig. S1). However, the expression levels of Cab39 mRNA and protein were increased greater in the livers of HFD-induced NASH mice compared to HFD- induced NAFLD (Figs. 4B and C, respectively). Based on these results, we investigated whether miR-451 directly regulates the Cab39 level in HepG2 cells transfected with miR-451 mimics by qRT-PCR and Western blot analyses. Our results showed that ectopic overexpression of miR-451 significantly reduced the expressed levels of Cab39. However, its expression level was not changed in miR-NC transfected cells ($p < 0.05$, Fig. 4D and E).

Together, these results demonstrated that the target sequence in the 3′-UTR of Cab39 (Fig. 4A) was regulated by miR-451 and this regulation could contribute to the negative correlation between endogenous miR-451 and Cab39 expression during NASH development.

3.6. *miR-451 inhibits PA-induced inflammation through the LKB1-AMPK pathway*

Cab39 functions as an armadillo repeat scaffolding-like protein that promotes LKB1 activity through stabilization of the LKB1/STRAD/Cab39 complex (Boudeau et al., 2004; Hawley et al., 2003; Taylor et al., 2006; Zeqiraj et al., 2009). To investigate the

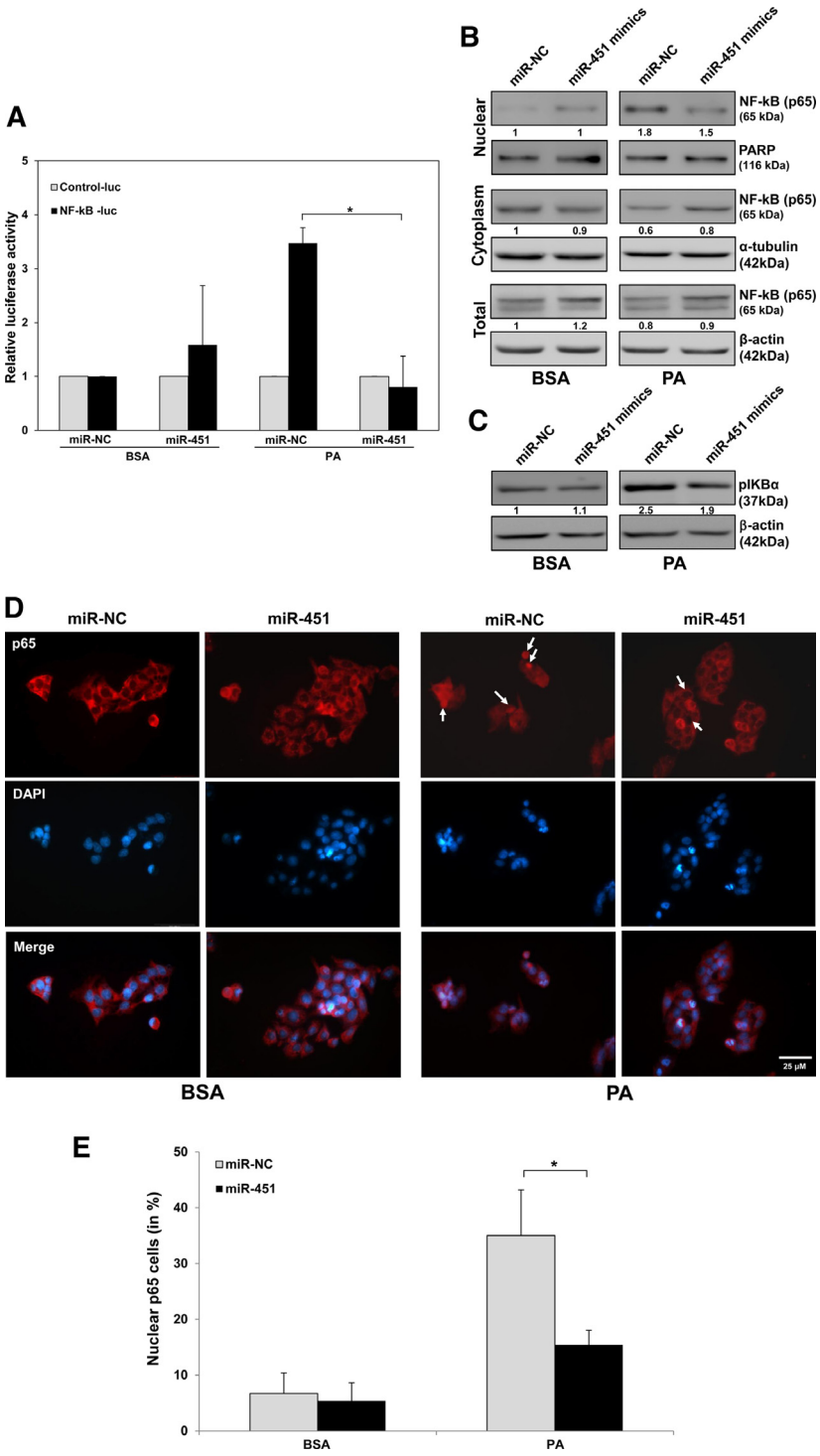

Fig. 3. Regulation of NF-κB signaling by miR-451 expression. (A) HepG2 cells were cotransfected with an NF-κB-Luc reporter plasmid or pGL3 luciferase reporter plasmid (Control-luc) and miR-451 mimics or a negative control pre-miRNA followed by exposure to PA or BSA. The HepG2 cells were also transfected with a vector containing *Renilla* luciferase to serve as a transfection efficiency control. After 6 h of PA or BSA treatment, cells were lysed and analyzed for luciferase expression using a dual-luciferase assay system. Results are expressed as the relative luciferase activity to the control vector. $^*P < 0.05$ compared from miR-NC. (B) HepG2 cells were harvested, and then prepared nuclear, cytosolic and whole cells extracts for the detection of NFκB p65 subunit. Western blot analysis shows the expression level of p65 in the nuclei, in the cytoplasm and in the whole cell in miR-451 expressing HepG2 cell with PA or BSA for 6 h. Summarized data ($n = 3$ experiments) show the average protein level of p65 (normalized to the protein level of PARP or α-tubulin or β-actin) corresponding to the bands shown in the Western blots. (C) Phosphorylated IκBα was assessed in total extracts by western blot. Results are expressed as ratio of p-IkB-a to β-actin. (D) HepG2 cells were stained with polyclonal anti- NF-κB p65 antibodies. The detection of NF-κB p65 with Cy3-conjugated secondary antibody (red) shows its distribution in the cytoplasm and nucleus of cells. The nuclei were counterstained with DAPI. An overlay of the images reveals the localization of NF-κB p65 proteins in the nucleus (purple). NF-κB p65 was located in the cytoplasm on miR-451 mimics or a negative control pre-miRNA followed by exposure to BSA (white arrow). NF-κB p65 translocated to nucleus after stimulated by PA (white arrow). miR-451 overexpression inhibited the translocation of NF-κB p65 into the nucleus after stimulated by PA (white arrow). These were observed by immunofluorescence. Magnification ×400. Scale bar = 25 μm. (E) Quantification of the effects of miR-451 expression on the translocation of p65. The translocation of p65 in 50–100 cells was analyzed. The percentage of cells with nuclear p65 is indicated, error bars represent SD (three experiments with at least 50 cells analyzed/condition and experiment), $^*P < 0.05$. (For interpretation of the references to color in this figure legend, the reader is referred to the web version of the article.)

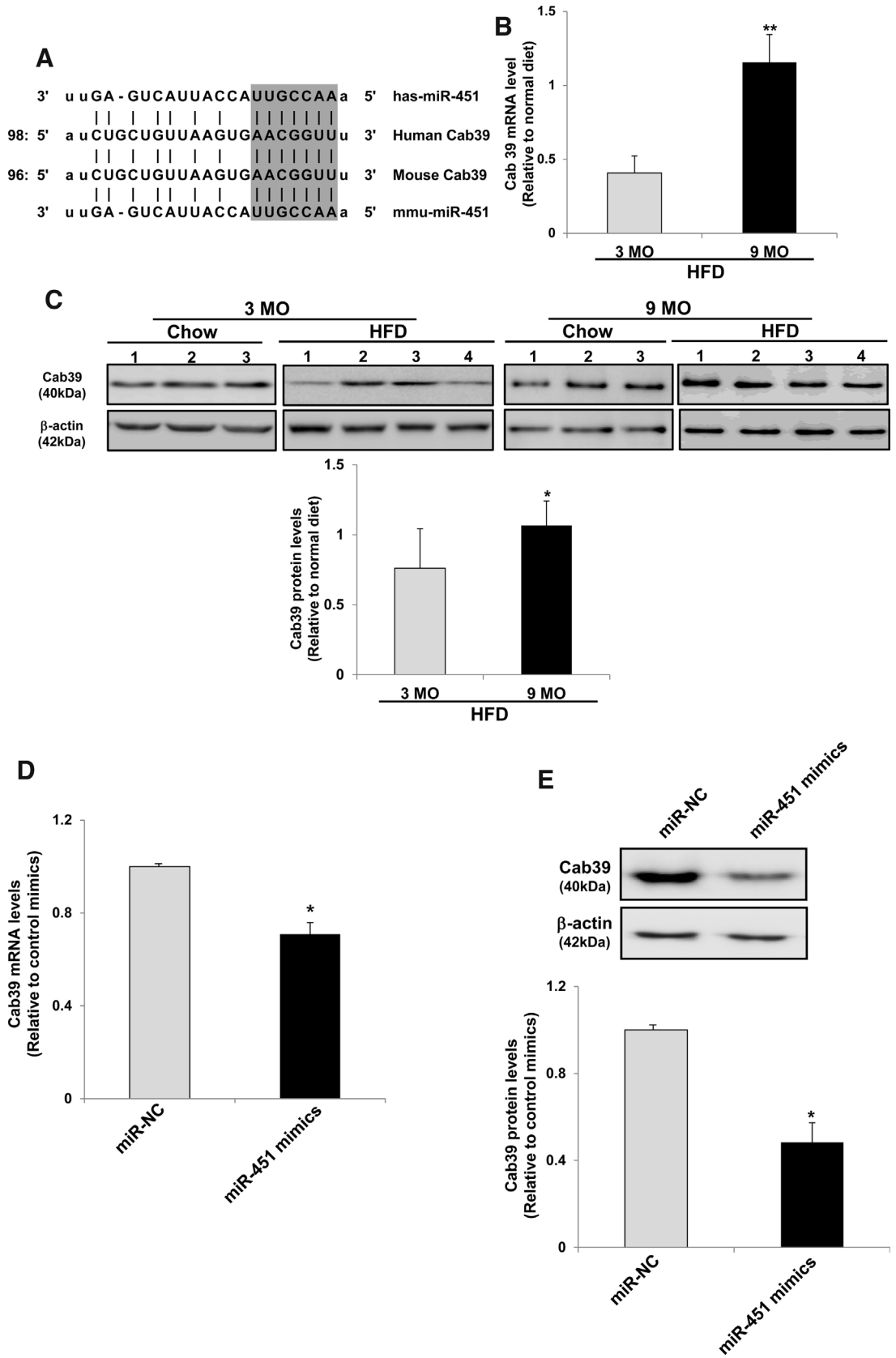

Fig. 4. Cab39 is a direct target of miR-451. (A) A conserved 7-mer target seed region (gray) of the miR-451 binding site was identified within the 3′ UTR of Cab39 in different mammalian species. (B) Real time analysis of Cab39 mRNA levels in livers from mice fed either regular chow ($n = 4$) or HFD for 3 months ($n = 4$) or 9 months ($n = 9$). $^*P < 0.05$ compared with 3 MO HFD. (C) Cab39 protein levels in livers from mice fed either regular chow ($n = 4$) or HFD for 3 months ($n = 4$) or 9 months ($n = 9$). $^*P < 0.05$ compared with 3 MO HFD. (D–E) HepG2 cells were transfected with miR-NC or miR-451 mimics. qRT-PCR (D) and immunoblot analyses (E) were performed 24 h after transfection to determine the Cab39 mRNA and protein levels, respectively, in transfected HepG2 cells. β-Actin was served as an internal control. $^*P < 0.05$ compared with miR-NC.

effect of miR-451 expression on LKB1/STRAD/Cab39 complex formation in HepG2 cells after PA exposure, we immunoprecipitated LKB1, followed by immunoblot analysis for LKB1, STRAD and Cab39. The overexpression of miR-451 substantially impaired the formation of a trimeric LKB1/STRAD/Cab39 complex in HepG2 cells treated with PA compared to BSA alone (Fig. 5A). These results indicate that miR-451 expression modulated the stabilization of the trimeric LKB1/STRAD/Cab39 in PA-induced steatotic HepG2 cells.

Based on these results, we hypothesized whether the effect of miR-451-mediated anti-inflammation was related

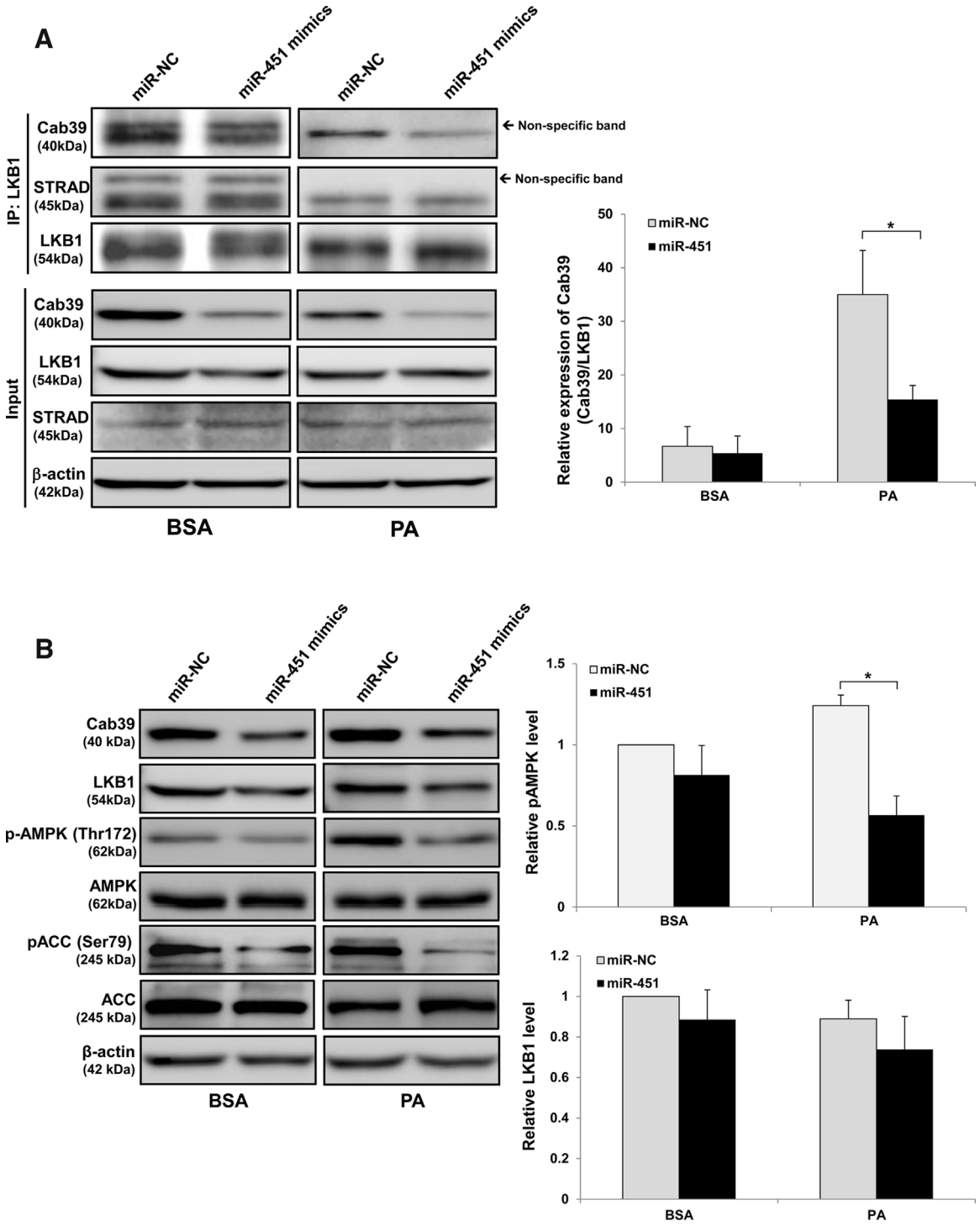

Fig. 5. Regulation of the LKB1/AMPK/AKT signaling pathway by miR-451 in PA- treated HepG2 cells. (A) Stabilization of the LKB1 complex by Cab39 as a target of miR-451. LKB1 was immunoprecipitated from the cell homogenates of PA-treated HepG2 cells transfected with miR-451 mimics or miR-NC followed by immunoblot analysis with anti-Cab39 or anti-STRAD antibodies. Input controls were blotted with anti-Cab39, anti-STRAD, anti-LKB1 antibodies and anti-β-actin antibody as indicated, while β-actin was used as a loading control. Quantification of the data shown in immunoprecipitation intensity was normalized to LKB1 immunoprecipitation. $^{*}P < 0.05$ compared with miR-NC. (B, C) Effect of miR-451 expression on AMPK phosphorylation and its downstream pathway. We performed immunoblot analysis to examine the levels of Cab39, LKB1, AMPK, ACC and AKT in miR-451-overexpressing cells after PA or BSA treatment. Band densities were quantified using TINA imaging analysis software and normalized to total AMPK, total ACC, total AKT or β-actin expression. $^{*}P < 0.05$ compared with miR-NC. (D) Western blotting was performed with cell extracts from BSA- or PA-treated HepG2 cells transfected with Cab39 siRNA or a scrambled siRNA.

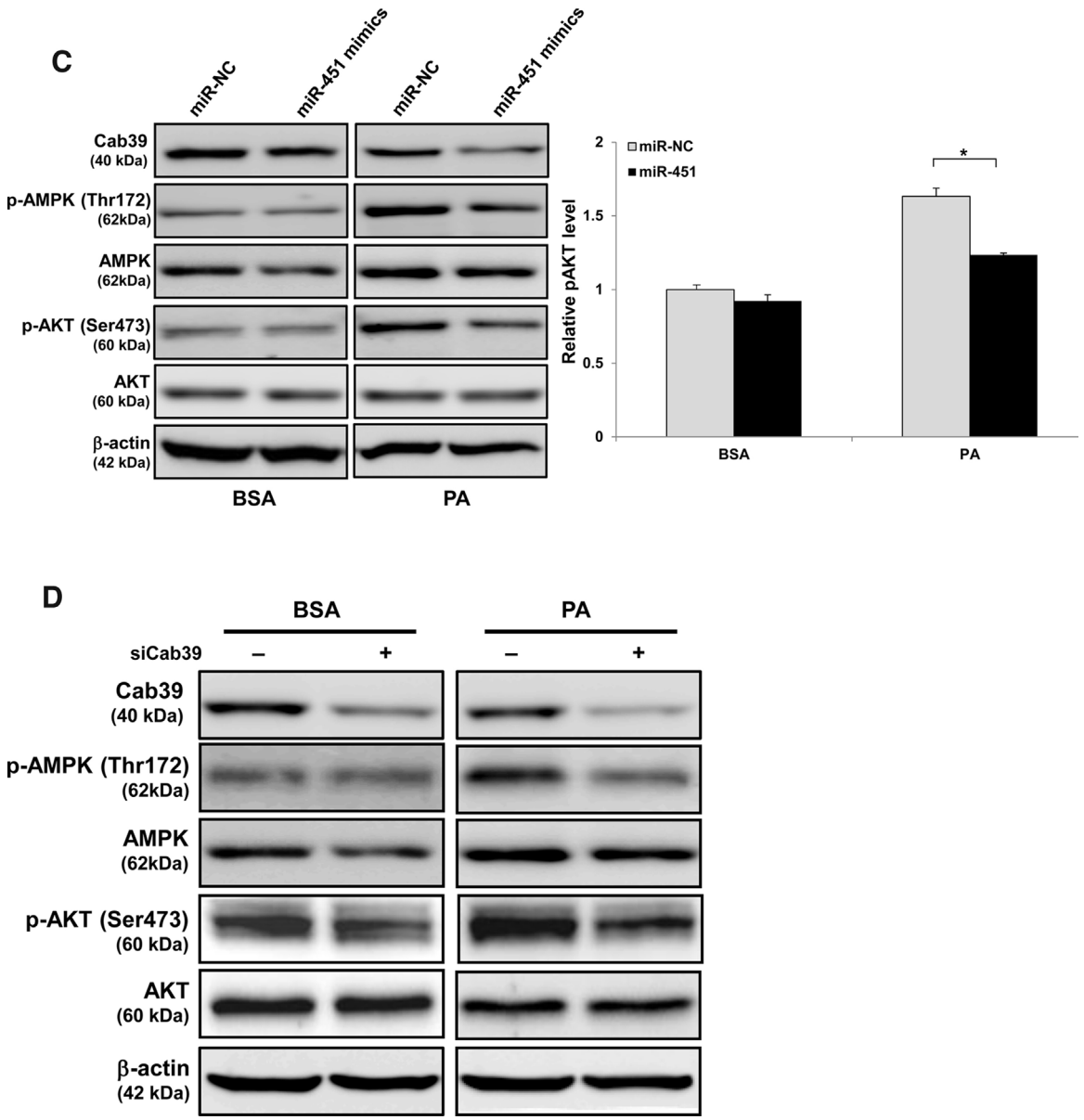

Fig. 5. (*Continued*)

to the AMPK/AKT pathway through stabilization of the LKB1/STRAD/Cab39 complex. To determine whether miR-451 expression inhibits PA-induced inflammation through blocking the AMPK/AKT pathway, we performed immunoblot analysis to measure the levels of Cab39, LKB1, AMPK Thr^{172} phosphorylation, ACC Ser^{79} phosphorylation and AKT Ser^{473} phosphorylation in miR-451-overexpressing cells treated with PA. As shown in Fig. 5B, overexpression of miR-451 in HepG2 cells treated with PA decreased LKB1, AMPK Thr^{172} phosphorylation and ACC Ser^{79} phosphorylation compared with miR-NC transfected HepG2 cells. The inhibition of AMPK phosphorylation led to decreased AKT phosphorylation (Fig. 5C). Similar to miR-451, silencing of Cab39 by the specific siRNA reduced the levels of AMPK phosphorylation and phosphorylated AKT in HepG2 cells treated with PA (Fig. 5D). In contrast, treatment of cells with a negative control siRNA did not alter the phosphorylation of AMPK and AKT, supporting the hypothesis of a miR-451-Cab39-AKT pathway. Collectively, these data demonstrate that miR-451 directly targets and down-regulates Cab39, resulting in inhibition of PA-induced inflammation through the AMPK/AKT pathway (Fig. 6).

4. Discussion

NAFLD, one of the most common causes of chronic liver disease (Lewis and Mohanty, 2010; Ogawa et al., 2014), is the result of excessive hepatic fat accumulation. The current understanding of the development and progression of NAFLD is encapsulated by a multistep process associated with hepatic steatosis, innate immune activation, inflammation, apoptosis and progressive liver damage. Our previous studies have shown that a mouse model of NAFLD, which was successfully established in C57BL/6 mice by HFD feeding exhibited morbid obesity with increased liver damage and collagen accumulation over time (Kim et al., 2014). In this study, the systematic investigation of cDNA expression profiling between hepatic steatosis and NASH was performed to explore the cellular mechanisms in the development of NASH. Among the significantly differentially expressed pathways, we focused on the roles of miR-451 during progression to NASH from simple steatosis. Consistent with a previous report (Alisi et al., 2011), our results showed that miR-451 expression was down-regulated in HFD-induced NASH mice (Fig. 2A) in liver tissue from human

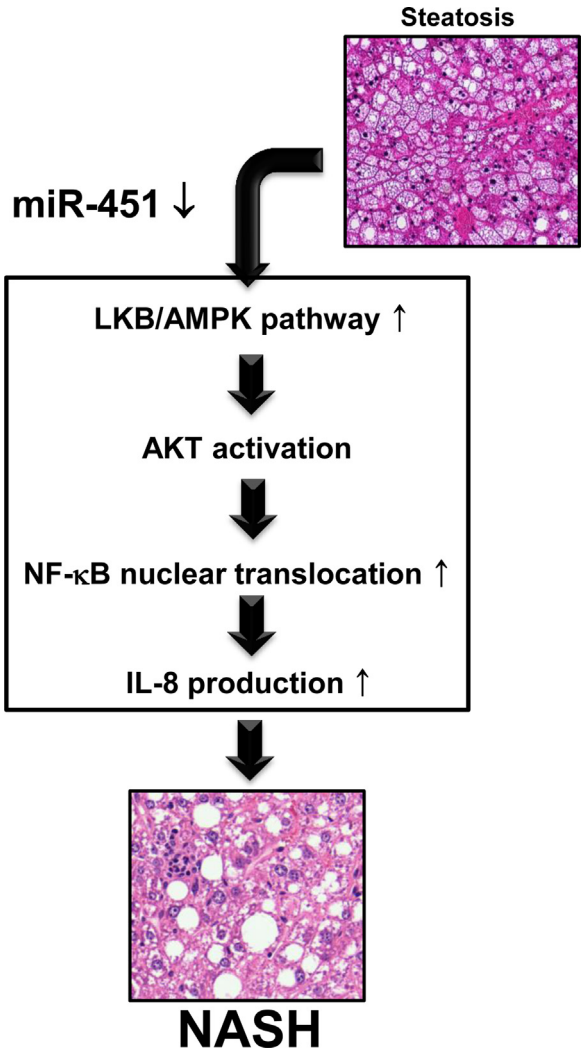

Fig. 6. Schematic diagram to show new negative regulation of miR-451 in the modulation of IL-8 expression during the progression of NAFLD *via* the AMPK/AKT/NF-κB pathway.

patients with NASH compared to those from patients with simple steatosis (Fig. 2C). These findings suggested that miR-451 plays an important role in the pathophysiological mechanisms involved the progression of NAFLD. Previously, many research groups have also demonstrated different biological functions for miR-451 in carcinogenesis and tumor progression by affecting cell proliferation, cell-cycle distribution, migration, and invasion (Bergamaschi and Katzenellenbogen, 2012; Gal et al., 2008; Li et al., 2013; Liu et al., 2013; Tian et al., 2012). In this study, we identified miR-451 as a NAFLD-expressed miRNA that regulates the production of inflammatory cytokines.

Among these proinflammatory cytokines, IL-8 functions as a critical chemoattractant and activator for neutrophils, basophils and T cells (Koch et al., 1992; Strieter et al., 1995). Many studies have shown that increased IL-8 expression is associated with several diseases, including NASH, obesity, diabetes, atherosclerosis, and various forms of liver injury (Kumar et al., 2012). Moreover, serum and hepatic levels of TNF-α in patient with NASH are increased and TNF-α levels correlate with histological severity (Dowman et al., 2010; Manco et al., 2007). These results suggest that proinflammatory cytokines, such as IL-8 or TNF-α play a key role in the development and/or progression of such metabolic diseases by promoting inflammation and tissue injury. In study, we employed an *in vitro* model of hepatic steatosis to investigate the molecular mechanisms linked to inflammatory processes associated with IL-8 and TNFα levels. We demonstrated that IL-8 and TNFα levels were significantly increased in HepG2 cells treated with free fatty acid PA. This suggests that IL-8 and TNFα expression induced by free fatty acid may play an important role in inflammatory liver injury and the progression of NAFLD. Furthermore, we demonstrated that NASH patients have significantly higher serum IL-8 and TNFα levels than healthy control group, suggesting an important role for IL-8 and TNFα in the pathogenesis of NASH (Supplementary Fig. S2). However, these IL-8 and TNFα expressions was significantly decreased in HepG2 cells treated with miR-451 mimics suggesting that miRNA-451 expression could negatively regulate inflammatory cytokine expressions in PA-exposed HepG2 cells. In this regard miR-451 may be a promising target molecule preventing the progression of NAFLD. Therefore, we further investigated the role and the molecular mechanism by which miR-451 promote the development of NASH from NAFLD. Our results showed that miR-451 regulates LKB1 activity through direct targeting of Cab39, a component of the active LKB1/STRAD/Cab39 complex. Disruption of LKB1 signaling by constitutive miR-451 expression alters the pathways downstream of LKB1 in steatotic cells. In addition, our results showed a reduced phosphorylation of AMPK and AKT in accordance with the decreased activation of NF-kB in response to PA treatment. These findings suggest that miR-451 plays an important role in the AMPK/AKT pathway during the progression of NAFLD. The partial Cab39 knockdown caused by miR-451 treatment led to marked destabilization of the LKB1/STRAD/CAB39 complex, as shown by co-immunoprecipitation results. These findings indicate that miR-451 overexpression is likely to have a potential inhibitory effect on the LKB1/AMPK/AKT signaling in steatotic cells (Fig. 6).

Our results offer new insight into the negative regulation of miR-451 in fatty acid-induced inflammation *via* the AMPK/AKT pathway and provide potential therapeutic applications for miR-451 in preventing the progression from simple steatosis to severe clinical liver disease.

Conflict of interest

The authors have declared that they have no potential conflicts of interest.

Acknowledgements

This research was partially supported by grants of Basic Science Research Program from the National Research Foundation of Korea (NRF) funded by the Ministry of Education, Science and Technology (2011-0014620 and 2012-001941) and the Korean Health Technology R&D Project, Ministry of Health & Welfare, Republic of Korea (no. 2011-08-0168-A0094).

References

Alisi A, Da Sacco L, Bruscalupi G, Piemonte F, Panera N, De Vito R, et al. Mirnome analysis reveals novel molecular determinants in the pathogenesis of diet-induced nonalcoholic fatty liver disease. Lab Invest 2011;91:283–93.

Bechmann LP, Hannivoort RA, Gerken G, Hotamisligil GS, Trauner M, Canbay A. The interaction of hepatic lipid and glucose metabolism in liver diseases. J Hepatol 2012;56:952–64.

Bellentani S, Marino M. Epidemiology and natural history of non-alcoholic fatty liver disease (NAFLD). Ann Hepatol 2009;8(Suppl. 1):S4–8.

Bergamaschi A, Katzenellenbogen BS. Tamoxifen downregulation of miR-451 increases 14-3-3zeta and promotes breast cancer cell survival and endocrine resistance. Oncogene 2012;31:39–47.

Bolstad BM, Irizarry RA, Astrand M, Speed TP. A comparison of normalization methods for high density oligonucleotide array data based on variance and bias. Bioinformatics 2003;19:185–93.

Boudeau J, Scott JW, Resta N, Deak M, Kieloch A, Komander D, et al. Analysis of the LKB1-STRAD-MO25 complex. J Cell Sci 2004;117:6365–75.

Castro RE, Ferreira DM, Afonso MB, Borralho PM, Machado MV, Cortez-Pinto H, et al. miR-34a/SIRT1/p53 is suppressed by ursodeoxycholic acid in the rat liver

and activated by disease severity in human non-alcoholic fatty liver disease. J Hepatol 2013;58:119–25.
Ceccarelli S, Panera N, Gnani D, Nobili V. Dual role of microRNAs in NAFLD. Int J Mol Sci 2013;14:8437–55.
Chae S, Ahn BY, Byun K, Cho YM, Yu MH, Lee B, et al. A systems approach for decoding mitochondrial retrograde signaling pathways. Sci Signal 2013;6:rs4.
Day CP, James OF. Steatohepatitis: a tale of two hits. Gastroenterology 1998;114:842–5.
Dowman JK, Tomlinson JW, Newsome PN. Pathogenesis of non-alcoholic fatty liver disease. QJM 2010;103:71–83.
Gal H, Pandi G, Kanner AA, Ram Z, Lithwick-Yanai G, Amariglio N, et al. MIR-451 and Imatinib mesylate inhibit tumor growth of Glioblastoma stem cells. Biochem Biophys Res Commun 2008;376:86–90.
Godlewski J, Nowicki MO, Bronisz A, Nuovo G, Palatini J, De Lay M, et al. MicroRNA-451 regulates LKB1/AMPK signaling and allows adaptation to metabolic stress in glioma cells. Mol Cell 2010;37:620–32.
Hawley SA, Boudeau J, Reid JL, Mustard KJ, Udd L, Makela TP, et al. Complexes between the LKB1 tumor suppressor, STRAD alpha/beta and MO25 alpha/beta are upstream kinases in the AMP-activated protein kinase cascade. J Biol 2003;2:28.
Huang da W, Sherman BT, Lempicki RA, Systematic. integrative analysis of large gene lists using DAVID bioinformatics resources. Nat Protoc 2009;4:44–57.
Hur W, Kim SW, Lee YK, Choi JE, Hong SW, Song MJ, et al. Oleuropein reduces free fatty acid-induced lipogenesis via lowered extracellular signal-regulated kinase activation in hepatocytes. Nutr Res 2012;32:778–86.
Hwang D, Rust AG, Ramsey S, Smith JJ, Leslie DM, Weston AD, et al. A data integration methodology for systems biology. Proc Natl Acad Sci USA 2005;102:17296–301.
Jeen YM, Jin SY. Pathology of nonalcoholic steatohepatitis. Korean J Hepatol 2009;15:122–30.
Joshi-Barve S, Barve SS, Amancherla K, Gobejishvili L, Hill D, Cave M, et al. Palmitic acid induces production of proinflammatory cytokine interleukin-8 from hepatocytes. Hepatology 2007;46:823–30.
Kim SW, Hur W, Li TZ, Lee YK, Choi JE, Hong SW, et al. Oleuropein prevents the progression of steatohepatitis to hepatic fibrosis induced by a high-fat diet in mice. Exp Mol Med 2014;46:e92.
Koch AE, Polverini PJ, Kunkel SL, Harlow LA, DiPietro LA, Elner VM, et al. Interleukin-8 as a macrophage-derived mediator of angiogenesis. Science 1992;258:1798–801.
Kumar R, Prakash S, Chhabra S, Singla V, Madan K, Gupta SD, et al. Association of pro-inflammatory cytokines, adipokines & oxidative stress with insulin resistance & non-alcoholic fatty liver disease. Indian J Med Res 2012;136:229–36.
Lewis JR, Mohanty SR. Nonalcoholic fatty liver disease: a review and update. Dig Dis Sci 2010;55:560–78.
Li HP, Zeng XC, Zhang B, Long JT, Zhou B, Tan GS, et al. miR-451 inhibits cell proliferation in human hepatocellular carcinoma through direct suppression of IKK-beta. Carcinogenesis 2013;34:2443–51.
Liu N, Jiang N, Guo R, Jiang W, He QM, Xu YF, et al. MiR-451 inhibits cell growth and invasion by targeting MIF and is associated with survival in nasopharyngeal carcinoma. Mol Cancer 2013;12:123.
Livak KJ, Schmittgen TD. Analysis of relative gene expression data using real-time quantitative PCR and the 2(−delta delta C(T)) method. Methods 2001;25:402–8.
Manco M, Marcellini M, Giannone G, Nobili V. Correlation of serum TNF-alpha levels and histologic liver injury scores in pediatric nonalcoholic fatty liver disease. Am J Clin Pathol 2007;127:954–60.
Murata K, Yoshitomi H, Furu M, Ishikawa M, Shibuya H, Ito H, et al. MicroRNA-451 down-regulates neutrophil chemotaxis via p38 MAPK. Arthritis Rheumatol 2014;66:549–59.
Nguyen TA, Sanyal AJ. Pathophysiology guided treatment of nonalcoholic steatohepatitis. J Gastroenterol Hepatol 2012;27(Suppl. 2):58–64.
Ogawa Y, Imajo K, Yoneda M, Nakajima A. Update: epidemiology and pathophysiology of nonalcoholic fatty liver disease. Nihon Shokakibyo Gakkai Zasshi 2014;111:14–24.
Pais R, Charlotte F, Fedchuk L, Bedossa P, Lebray P, Poynard T, et al. A systematic review of follow-up biopsies reveals disease progression in patients with non-alcoholic fatty liver. J Hepatol 2013;59:550–6.
Park S, Choi Y, Um SJ, Yoon SK, Park T. Oleuropein attenuates hepatic steatosis induced by high-fat diet in mice. J Hepatol 2011;54:984–93.
Pogribny IP, Starlard-Davenport A, Tryndyak VP, Han T, Ross SA, Rusyn I, et al. Difference in expression of hepatic microRNAs miR-29c, miR-34a, miR-155, and miR-200b is associated with strain-specific susceptibility to dietary nonalcoholic steatohepatitis in mice. Lab Invest 2010;90:1437–46.
Rosenberger CM, Podyminogin RL, Navarro G, Zhao GW, Askovich PS, Weiss MJ, et al. miR-451 regulates dendritic cell cytokine responses to influenza infection. J Immunol 2012;189:5965–75.
Shukla GC, Singh J, Barik S. MicroRNAs: processing, maturation, target recognition and regulatory Functions. Mol Cell Pharmacol 2011;3:83–92.
Strieter RM, Polverini PJ, Arenberg DA, Kunkel SL. The role of CXC chemokines as regulators of angiogenesis. Shock 1995;4:155–60.
Targher G, Day CP, Bonora E. Risk of cardiovascular disease in patients with nonalcoholic fatty liver disease. N Engl J Med 2010;363:1341–50.
Taylor EB, Ellingson WJ, Lamb JD, Chesser DG, Compton CL, Winder WW. Evidence against regulation of AMP-activated protein kinase and LKB1/STRAD/MO25 activity by creatine phosphate. Am J Physiol Endocrinol Metab 2006;290:E661–9.
Tian Y, Nan Y, Han L, Zhang A, Wang G, Jia Z, et al. MicroRNA miR-451 down-regulates the PI3K/AKT pathway through CAB39 in human glioma. Int J Oncol 2012;40:1105–12.
Tilg H, Moschen AR. Evolution of inflammation in nonalcoholic fatty liver disease: the multiple parallel hits hypothesis. Hepatology 2010;52:1836–46.
Wang SL, Li Y, Wen Y, Chen YF, Na LX, Li ST, et al. Curcumin, a potential inhibitor of up-regulation of TNF-alpha and IL-6 induced by palmitate in 3T3-L1 adipocytes through NF-kappaB and JNK pathway. Biomed Environ Sci 2009;22:32–9.
Wu LN, Wei XW, Fan Y, Miao JN, Wang LL, Zhang Y, et al. Altered expression of 14-3-3zeta protein in spinal cords of rat fetuses with spina bifida aperta. PLoS ONE 2013;8:e70457.
Zeqiraj E, Filippi BM, Deak M, Alessi DR, van Aalten DM. Structure of the LKB1-STRAD-MO25 complex reveals an allosteric mechanism of kinase activation. Science 2009;326:1707–11.
Zhang Z, Luo X, Ding S, Chen J, Chen T, Chen X, et al. MicroRNA-451 regulates p38 MAPK signaling by targeting of Ywhaz and suppresses the mesangial hypertrophy in early diabetic nephropathy. FEBS Lett 2012;586:20–6.